STRUCTURAL CHEMISTRY

ISSN 2053-2296

Crystal and molecular structures of *fac*-[Re(Bid)-(PPh_3)($(CO)_3$)] [Bid is tropolone (TropH) and tribromotropolone ($TropBr_3H$)]

Marietjie Schutte-Smith* and Hendrik Gideon Visser

Department of Chemistry, University of the Free State, PO Box 339, Bloemfontein 9301, South Africa. *Correspondence e-mail: schuttem@ufs.ac.za

Received 30 November 2021
Accepted 2 May 2022

Edited by S. Moggach, The University of Western Australia, Australia

Keywords: tropolone; triphenylphosphane; crystal structure; solid-state NMR spectroscopy; Hirshfeld analysis.

CCDC references: 2108567; 2108568

Supporting information: this article has supporting information at journals.iucr.org/c

Two rhenium complexes, namely, *fac*-tricarbonyl(triphenylphosphane-κP)(tropolonato-$\kappa^2 O,O'$)rhenium(I), $[Re(C_7H_5O_2)(C_{18}H_{15}P)(CO)_3]$ or *fac*-[Re(Trop)-(PPh_3)$(CO)_3$] (**1**), and *fac*-tricarbonyl(3,5,7-tribromotropolonato-$\kappa^2 O,O'$)(triphenylphosphane-κP)rhenium(I), $[Re(C_7H_2Br_3O_2)(C_{18}H_{15}P)(CO)_3]$ or *fac*-[Re($TropBr_3$)(PPh_3)$(CO)_3$] (**2**) (TropH is tropolone and and $TropBr_3H$ is tribromotropolone), were synthesized and their crystal and molecular structures confirmed by single-crystal X-ray diffraction. Both crystallized in the space group $P\overline{1}$ and display an array of inter- and intramolecular interactions which were confirmed by solid-state ^{13}C NMR spectroscopy using cross polarization magic angle spinning (CPMAS) techniques, as well as Hirshfeld surface analysis. The slightly longer Re—P distance of **1** [2.4987 (5) *versus* 2.4799 (11) Å for **1** and **2**, respectively] suggests stronger back donation from the carbonyl groups in the former case, possibly due to the stronger electron-donating ability of the unsubstituted tropolonate ring system. However, this is not supported in the Re—CO bond distances of **1** and **2**.

1. Introduction

Rhenium(I) tricarbonyl complexes not only have application as models for similar technetium(I) complexes in radiopharmacy, but their anticancer and antimicrobial properties have recently been investigated by several research groups, including ours (Gantsho *et al.*, 2020; Collery *et al.*, 2019; Li *et al.*, 2012; Otero *et al.*, 2019; Leonidova & Gasser, 2014; Brink *et al.*, 2018; Sovari *et al.*, 2020, 2021; Varma *et al.*, 2020). Similarly, the bidentate ligand tropolone and its derivatives have shown anticancer and antiviral properties on their own (Ishihara *et al.*, 2010; Borowski *et al.*, 2007; Dittes *et al.*, 1995*a*) and when combined with metal complexes (Ishihara *et al.*, 2010; Borowski *et al.*, 2007; Dittes *et al.*, 1995*a*,*b*; Trust, 1975). Kinetic studies have shown that tropolone and other *O*,*O*′-bidentate ligands like 3-hydroxyflavone increase the rate of substitution of water or methanol in *fac*-[Re(Bid)$X$$(CO)_3$]^n (Bid = bidentate ligand, X = H_2O or methanol, and n = 0 or 1+) type complexes by up to 20000 times (Gantsho *et al.*, 2020; Schutte *et al.*, 2012; Schutte-Smith *et al.*, 2019*b*; Schutte *et al.*, 2011; Manicum *et al.*, 2020; Schutte-Smith & Visser, 2015). This kind of mechanistic information is extremely important when designing molecules for anticancer, antibacterial and antiviral applications, as well as in radiopharmacy (Collery *et al.*, 2019; Schutte-Smith *et al.*, 2019*b*). Recently, we showed that kinetic data can be correlated with cytotoxicity and cell availability (Schutte-Smith *et al.*, 2020).

Our focus is to try to understand the basic chemistry (mechanism of action, structure–activity relationships and

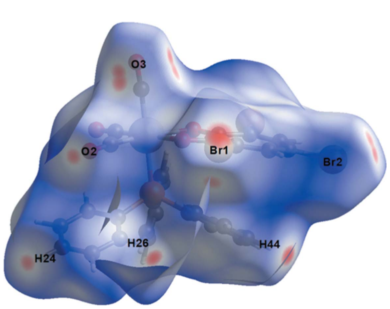

 https://doi.org/10.1107/S205322962200465X

Table 1
Experimental details.

For both structures: triclinic, $P\overline{1}$, $Z = 2$. Experiments were carried out with Mo $K\alpha$ radiation using a Bruker D8 Quest Eco Chi Photon II CPAD diffractometer for **1** and a Bruker D8 Venture 4K Kappa Photon III C28 diffractometer for **2**. Absorption was corrected for by multi-scan methods (*SADABS*; Bruker, 2012). H-atom parameters were constrained.

	1	**2**
Crystal data		
Chemical formula	$[Re(C_7H_5O_2)(C_{18}H_{15}P)(CO)_3]$	$[Re(C_7H_2Br_3O_2)(C_{18}H_{15}P)(CO)_3]$
M_r	653.61	890.32
Temperature (K)	100	104
a, b, c (Å)	9.9301 (11), 10.1686 (10), 12.7882 (14)	8.5413 (12), 8.7024 (13), 20.376 (3)
α, β, γ (°)	80.948 (3), 71.899 (3), 88.682 (3)	102.221 (5), 93.891 (5), 109.093 (5)
V (Å^3)	1211.6 (2)	1383.3 (3)
μ (mm^{-1})	5.12	8.82
Crystal size (mm)	0.27 × 0.17 × 0.13	0.18 × 0.04 × 0.04
Data collection		
T_{min}, T_{max}	0.357, 0.511	0.690, 0.728
No. of measured, independent and observed [$I > 2\sigma(I)$] reflections	25538, 5820, 5726	34880, 6818, 5913
R_{int}	0.037	0.068
$(\sin \theta/\lambda)_{max}$ (Å^{-1})	0.661	0.668
Refinement		
$R[F^2 > 2\sigma(F^2)]$, $wR(F^2)$, S	0.015, 0.038, 1.08	0.029, 0.062, 1.06
No. of reflections	5820	6818
No. of parameters	316	343
$\Delta\rho_{max}$, $\Delta\rho_{min}$ (e Å^{-3})	0.46, −0.60	0.93, −1.49

Computer programs: *APEX2* (Bruker, 2012), *SAINT-Plus* (Bruker, 2012), *SHELXT* (Sheldrick, 2015*a*), *SHELXL2018* (Sheldrick, 2015*b*), *WinGX* (Farrugia, 2012) and *DIAMOND* (Brandenburg & Putz, 2019).

stability) of these organometallic compounds to aid in the design of new bioactive pharmaceuticals. This also includes the characterization by means of solid- and solution-state multinuclear NMR spectroscopy, single-crystal X-ray diffraction and other spectroscopic methods. The application of solid-state NMR spectroscopy to study hydrogen-bond and other intra- and intermolecular interactions is growing rapidly, with many research groups involved in the development of new techniques to study crystalline and even amorphous phases, making it a useful tool for our purposes as well (Chierotti & Gobetto, 2008; Traer *et al.*, 2007; Zhao *et al.*, 2001; Schutte-Smith *et al.*, 2019*a*; Wilhelm *et al.*, 2022).

We report here the crystal and molecular structures of *fac*-$[Re(Trop)(PPh_3)(CO)_3]$ (**1**) and *fac*-$[Re(TropBr_3)(PPh_3)(CO)_3]$ (**2**) (TropH is tropolone and $TropBr_3H$ is tribromotropolone), together with the solid- and solution-state multinuclear NMR spectroscopic analysis, and we attempt to correlate the spectral data with bond lengths and interactions.

2. Experimental

2.1. Materials and methods

All reagents employed in the preparation and characterization of the title compounds were of analytical grade, were purchased from Sigma–Aldrich or Merck (South Africa) and were used without any further purification; all experiments were performed aerobically. The IR spectra were recorded at room temperature on a PerkinElmer BX II IR spectrometer in the range 4000–370 cm^{-1}.

The liquid-state ^{1}H, ^{13}C and ^{31}P NMR spectra were recorded at 25.0 °C on a 300 MHz Bruker Fourier NMR spectrometer, a 400 MHz Avance III NMR spectrometer and a 600 MHz Avance II Bruker spectrometer, respectively, and methanol-d_4, toluene-d_6 and acetone-d_6 were used as solvents. The chemical shifts (δ) are reported in parts per million (ppm); for methanol-d_4 and acetone-d_6, the spectra were referenced relative to the solvent peak (3.31 ppm for ^{1}H and 49.15 ppm for ^{13}C, and 2.05 for ^{1}H and 29.92 for ^{13}C, respectively). Coupling constants (J) are reported in Hz. The solid-state NMR spectra were collected on a 400 MHz Bruker Avance III spectrometer equipped with a 4 mm VTN multinuclear double resonance magic angle spinning probe, operating at 25.0 °C. The ^{13}C NMR spectra were recorded at 100.6 MHz, using the cross polarization magic angle spinning (CP/MAS) technique. A rotating speed of 10000 Hz was used with a contact time of 2 ms, a recycle delay of 5 s and an acquisition time of 33.9 ms. All the spectra were recorded with 3k scans. The samples were packed in 4 mm zirconia rotors.

2.2. Synthesis and crystallization

2.2.1. *fac*-$[Re(Trop)(PPh_3)(CO)_3]$ (1). *fac*-$[Re(Trop)(CO)_3(H_2O)]$ (50 mg, 0.122 mmol), synthesized according to a previously reported procedure (Schutte *et al.*, 2012), was dissolved in acetone (30 ml) and triphenylphosphane (32 mg, 0.122 mmol) was added to the solution. The mixture was stirred overnight at room temperature and left to crystallize from the acetone solution (yield: 69 mg, 87%).

IR (KBr, cm^{-1}): ν_{CO} = 2010, 1934, 1887. ^{1}H NMR (400.13 MHz, acetone-d_6): δ 7.42 (*m*, 15H), 7.23 (*t*, 2H, J = 10.6 Hz), 6.91 (*d*, 2H, J = 10.8 Hz), 6.84 (*t*, 1H, J = 9.6 Hz). ^{13}C NMR (100.61 MHz, acetone-d_6): δ 184 (Trop), 138 (Trop), 134

(PPh$_3$), 131 (PPh$_3$), 129 (PPh$_3$), 127 (Trop). ^{13}C CP/MAS NMR (100.61 MHz): δ 183, 182, 138, 136, 135, 133, 132, 130, 129, 128, 127, 126. ^{31}P (161.97 MHz, acetone-d_6): δ 18.2. Analysis calculated (%): C 51.45, H 3.08, P 4.74; found: C 51.43, H 3.11, P 1.76.

2.2.2. *fac*-[Re(TropBr$_3$)(PPh$_3$)(CO)$_3$] (2). *fac*-[Re(TropBr$_3$)(CO)$_3$(H$_2$O)] (50 mg, 0.077 mmol), synthesized according to a previously reported procedure (Schutte *et al.*, 2008), was dissolved in acetone (30 ml) and triphenylphosphane (20 mg, 0.0077 mmol) was added to the solution. The mixture was stirred overnight at room temperature and left to crystallize from the acetone solution (yield: 62.5 mg, 91%).

IR (KBr, cm^{-1}): ν_{CO} = 2018, 1922, 1889. ^{1}H NMR (400.13 MHz, acetone-d_6): δ 8.15 (s, 2H), 7.42 (m, 15H). ^{13}C NMR (150.95 MHz, acetone-d_6): δ 176 (Trop), 143 (Trop), 134 (PPh$_3$), 132 (Trop), 129 (Trop). ^{13}C CP/MAS NMR (100.61 MHz): δ 135, 133, 131, 129. ^{31}P (161.97 MHz, acetone-d_6): δ 19.6. Analysis calculated (%): C 37.77, H 1.92, P 3.48; found: C 37.81, H 1.90, P 3.45.

2.3. Refinement

Crystal data, data collection and structure refinement details are summarized in Table 1. All aromatic H atoms were placed in geometrically idealized positions (C—H = 0.95 Å) and constrained to ride on their parent atoms, with U_{iso}(H) = 1.2U_{eq}(C).

3. Results and discussion

3.1. Synthesis

fac-[Re(Trop)(PPh$_3$)(CO)$_3$] (**1**) and *fac*-[Re(TropBr$_3$)(PPh$_3$)(CO)$_3$] (**2**) were synthesized from the respective aqua complexes, which were synthesized according to previously reported procedures (Gantsho *et al.*, 2020; Schutte *et al.*, 2008, 2012). The synthesis of **1** was described previously, but crystals suitable for single-crystal X-ray diffraction could not be obtained at the time (Gantsho *et al.*, 2020). Compounds **1** and **2** were synthesized in good yield from acetone solutions, after stirring the respective aqua complexes with one equivalent of triphenylphoshane overnight.

Table 2
Selected geometric parameters (Å, °) for **1**.

Re1—C1	1.900 (2)	Re1—O12	2.1322 (13)
Re1—C2	1.912 (2)	Re1—O11	2.1345 (13)
Re1—C3	1.944 (2)	Re1—P1	2.4987 (5)
O12—Re1—O11	73.99 (5)	O12—Re1—P1	88.10 (4)
C3—Re1—P1	177.15 (6)	O11—Re1—P1	86.59 (4)

In the ^{1}H NMR spectra, a significant downfield shift is observed from **1** (7.23, 6.91 and 6.84 ppm) to **2** (8.15 ppm) for the tropolonate and tribromotropolonate H atoms, respectively, which is expected due to the electron-withdrawing Br atoms in **2** causing deshielding of the nuclei. This is confirmed in the ^{31}P NMR spectra with a slight downfield shift in the phosphorus peak of **1** at 18.2 ppm and **2** at 19.6 ppm. The IR carbonyl stretching frequencies of **1** (2010, 1934 and 1887 cm^{-1}) are lower than **2** (2018, 1922 and 1889 cm^{-1}), which is expected since the tropolonate ligand in **1** is more electron donating than the tribromotropolonate ligand in **2**, therefore implying stronger backbonding from the carbonyl ligands to the metal centre and resulting in lower CO stretching frequencies. This, in turn, labilizes the phosphane ligand in the sixth position and is confirmed in the solid-state structures, with the Re—P bond lengths reported as 2.4987 (5) Å for **1** and 2.4799 (11) Å for **2**.

3.2. X-ray crystallography

A summary of the crystal data for **1** and **2** is given in Table 1. *fac*-[Re(Trop)(PPh$_3$)(CO)$_3$], **1**, crystallized in the triclinic space group $P\overline{1}$ with one molecule in the asymmetric unit. The molecular diagram and selected bond lengths and angles are given in Fig. 1 and Table 2, respectively. Three intermolecular

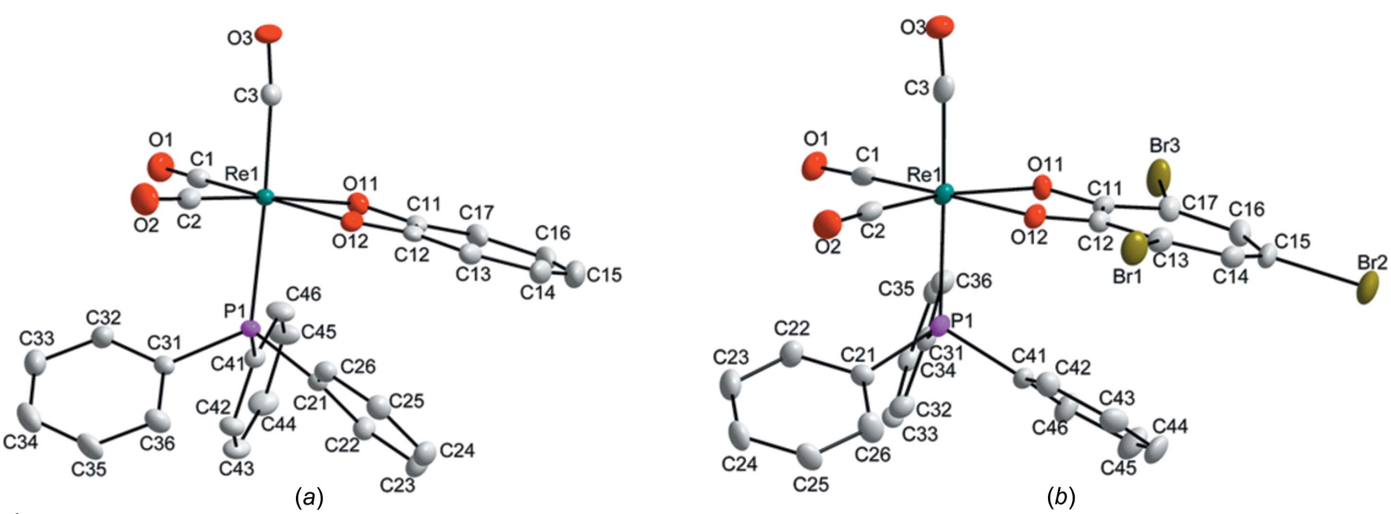

Figure 1
The molecular structures of (*a*) *fac*-[Re(Trop)(PPh$_3$)(CO)$_3$] (**1**) and (*b*) *fac*-[Re(TropBr$_3$)(PPh$_3$)(CO)$_3$] (**2**), showing the atom-numbering schemes. H atoms have been omitted for clarity. Displacement ellipsoids are drawn at the 50% probability level.

Table 3
Selected geometric parameters (Å, °) for **2**.

Re1—C2	1.903 (4)	Re1—O12	2.127 (3)
Re1—C1	1.917 (4)	Re1—O11	2.159 (2)
Re1—C3	1.950 (5)	Re1—P1	2.4799 (11)
O12—Re1—O11	73.05 (10)	C12—O12—Re1	118.7 (2)
C3—Re1—P1	176.09 (11)	C11—O11—Re1	117.4 (2)

and one intramolecular hydrogen-bonding interaction (C—H···O) are observed in the structure, as well as two intermolecular C—O···π and one intramolecular π–π interaction (Figs. S1 and S2 in the supporting information). A summary of the geometric parameters of these interactions is given in Tables S1 and S2 in the supporting information. Interestingly, the hydrogen-bond interactions involve the tropolonate ligand and the C atoms of the C41-ring as C—H donor atoms, and the O atoms of the tropolonate ring and the O atom of a carbonyl ligand as acceptor atoms. The π-interactions, on the other hand, involve interactions between the carbonyl O2 and O3 atoms and the centroids of the five-membered Re/O11/C11/C12/O12 ring, as well as the arene rings of the phosphane ligand (C21–C26 and C31–C36).

fac-[Re(TropBr$_3$)(PPh$_3$)(CO)$_3$], **2**, also crystallized in the triclinic space group $P\overline{1}$ with one molecule in the asymmetric unit. The molecular diagram is given in Fig. 1 and selected bond lengths and angles are provided in Table 3. Four intermolecular hydrogen-bond interactions (three C—H···O and one C—H···Br) and one intramolecular hydrogen-bond interaction (C—H···O) are observed in the structure of **2** (Fig. S3 in the supporting information). A short contact of 3.250 (4) Å is observed between Br2 and O3($-x + 1$, $-y + 1$, $-z + 1$) (Fig. S4). Two intermolecular contacts form an infinite one-dimensional chain with base vector [110] between Br1 and Br3($x - 1$, $y - 1$, z), and between Br3 and Br1($x + 1$, $y + 1$, z), both with a distance of 3.4809 (7) Å (Fig. S5). A range of π-interactions are observed: one X—H···π, two π–π and three Y—X···π interactions ranging between 3.438 (4) and 3.865 (2) Å (Fig. S4). A summary of the geometric parameters of these interactions is given in Tables S3 and S4 in the supporting information. All three Br atoms are involved in short contacts, while Br2 is additionally involved in a π-interaction and Br3 is involved as an acceptor in a hydrogen-bond interaction. All five of the ring systems, *i.e.* the three arene rings of the PPh$_3$ ligand, the tropolonate ring and the Re1/O11/C11/C12/O12 five-membered ring, are involved in the π-interactions.

The bond lengths and angles of **1** and **2** compare well with each other and also with similar structures in the literature (Gantsho *et al.*, 2020; Schutte-Smith *et al.*, 2019*b*; Schutte *et al.*, 2007, 2008; Manicum *et al.*, 2020; Bochkova *et al.*, 1987; Kydonaki *et al.*, 2016). The Re—P1 bond length of **1** is slightly longer than in **2**, possibly due to the electron-withdrawing effect of the three Br atoms on the backbone of **2**. The tropolonate ligand in **1** donates more electron density to the rhenium metal centre, initiating more backbonding from the

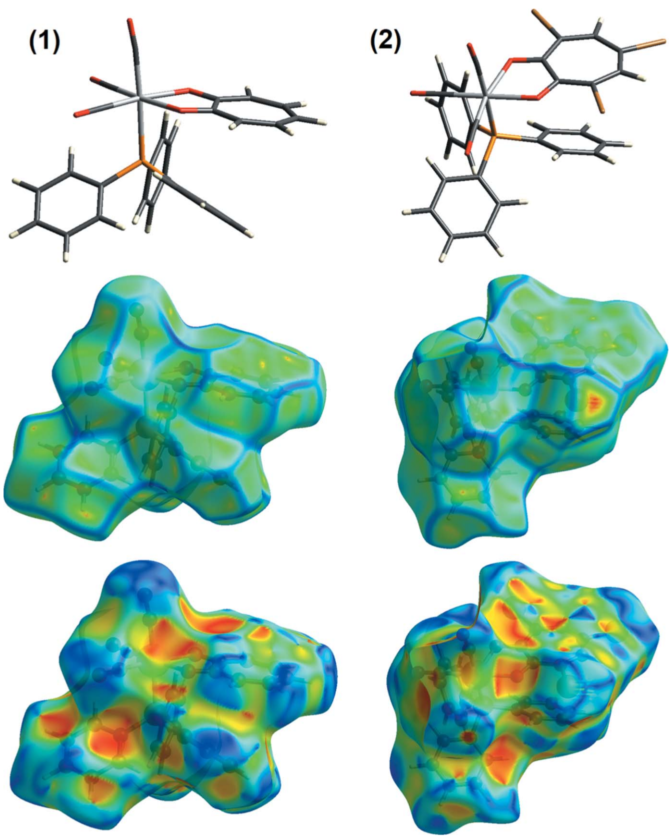

Figure 2
The Hirshfeld surfaces of **1** and **2**, illustrating a curvedness plot (middle), a shape index plot (bottom) and the molecular diagram for clarity of **1** and **2**.

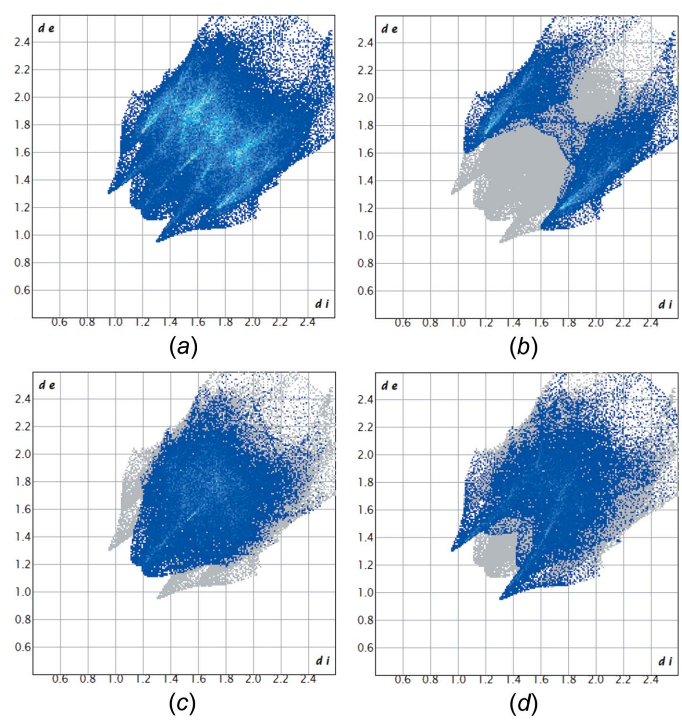

Figure 3
Fingerprint plots of **1**: (*a*) full plot with the total Hirshfeld surface area of the molecules. Fingerprint plots of **1** resolved into (*b*) H···C/C···H (26.5%), (*c*) H···H (38.1%) and (*d*) O···H/H···O (28%).

Table 4
Comparison of bond lengths (Å) of *fac*-[Re(Trop)(PPh_3)$(CO)_3$] (**1**) and [Re(Trop)$(PPh_3)_2(CO)_2$] (**3**).

Bond	1	3
Re1—C1	1.900 (2)	1.883 (3)
Re1—C2	1.912 (2)	1.887 (3)
Re1—O11	2.1345 (13)	2.1578 (19)
Re1—O12	2.1322 (13)	2.1548 (18)
Re1—P1	2.4987 (5)	2.4302 (8)
Re1—P2		2.4239 (8)

carbonyl ligands, labilizing the Re—P bond. Although this is what we expect, it is not observed in the Re—CO bond lengths of **1** and **2**, which do not differ significantly. Considering the angles around the Re^{I} metal core, a good correlation between **1** and **2** is found. The small bite angles of 73.99 (5) and 73.05 (10)° for **1** and **2**, respectively, indicate the degree of distortion of the octahedral geometry, which is normal and within the range of other similar structures where a five-membered *O*,*O*′-chelate ring is formed with the metal centre (Gantsho *et al.*, 2020; Schutte *et al.*, 2007, 2008; Schutte-Smith *et al.*, 2019*b*; Bochkova *et al.*, 1987). In the case of a six-membered *O*,*O*′-chelate ring (with PPh_3 in the sixth position), the bite angle is slightly larger, with values ranging between 82.2 and 84.7° (Manicum *et al.*, 2020; Kydonaki *et al.*, 2016).

The tropolonate and tribromotropolonate ligands bend slightly towards the triphenylphosphane ligand in **1** and **2**, with dihedral angles between the plane through the $Re(CO)_3$ entity and the ligand (the plane through Re/C1/O1/C2/O2 and the plane through O11/O12/C11–C17) of 8.85 (8) and 12.43 (14)°, respectively (illustrated in Fig. S6 in the supporting information). In **2**, the Br atoms are slightly 'out of plane' with respect to the tropolonate ring (C11–C17) at −0.1463 (4), 0.1760 (5) and −0.2114 (5) Å for Br1, Br2 and Br3, respectively. This could be due to the different interactions observed: the intermolecular contacts between Br1 and Br3 and the C—H···Br3 hydrogen-bond interaction, and the Br2···O3 short contact and C15—Br2···*Cg*1($-x+1, -y+1, -z+1$) π-interaction for Br2 (*Cg*1 is the centroid of the Re/C1/O1/C2/O2 ring).

The Hirshfeld surfaces of **1** and **2** are illustrated in Fig. 2 (Spackman & Jayatilaka, 2009). The molecular diagram of the compound is given at the top of the figure to illustrate the orientation of each compound in the curvedness (middle) and shape index (bottom) plots below it. In **1**, the blue concave regions around O2 and O3 correspond to the C2—O2···*Cg*3-($-x+2, -y, -z+1$) (*Cg*3 is the centroid of the C31–C36 ring) and C3—O3···*Cg*1($-x+2, -y, -z$) *Y*—*X*···π interactions as given in Table S2 (see supporting information), while a red convex region around O1 corresponds to the C17—H17···O1-($-x+2, -y+1, -z$) hydrogen-bond interaction (Table S1). The large red convex area above the rhenium five-membered ring and atoms O11 and O12 correlates with the three hydrogen-bond interactions C44—H44···O12($x, y+1, z$), C45—H45···O11($-x+2, -y+1, -z$) and C46—H46···O11, and the π-interaction C3—O3···*Cg*1($-x+2, -y, -z$) (Table S1 and Table S2).

In **2**, the blue and red adjacent triangles above the tribromotropolonate ring system correlate with the π–π interactions given in Table S4 (Seth *et al.*, 2011). Blue convex regions are observed around the donor atoms Br1, Br2 and Br3 [C15—Br2···*Cg*1($-x+1, -y+1, -z+1$), Br1···Br3-($x-1, y-1, z$), Br3···Br1($x+1, y+1, z$) and Br2···O3-($-x+1, -y+1, -z+1$)], as well as red concave regions above

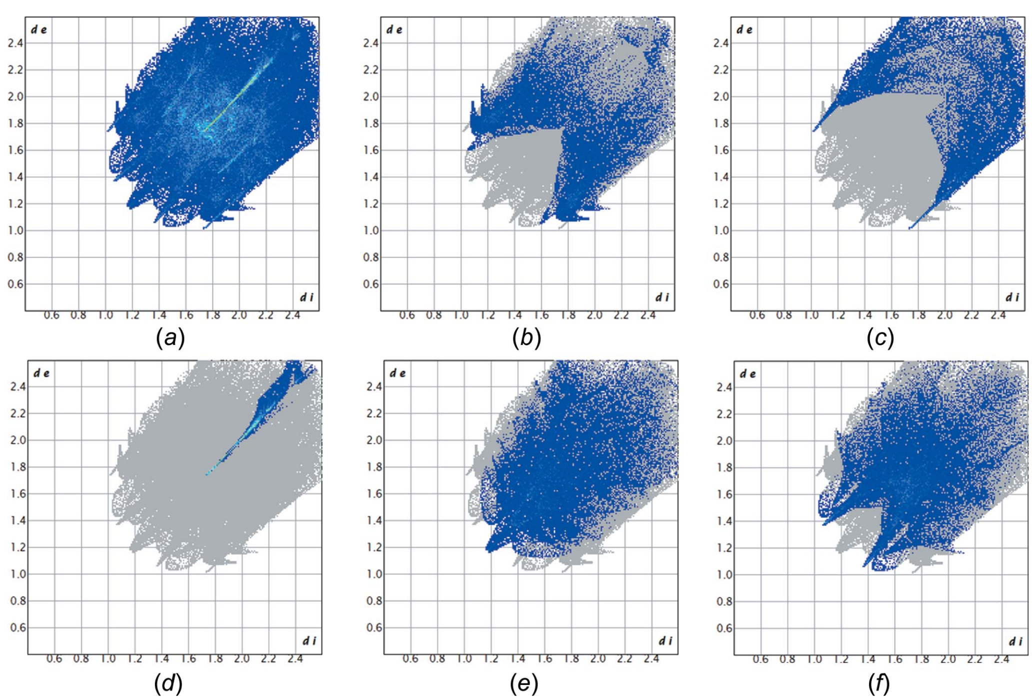

Figure 4
Fingerprint plots of **2**: (*a*) full plot with the total Hirshfeld surface area of the molecules. Fingerprint plots of **2** resolved into (*b*) C···H/H···C (16%), (*c*) Br···H/H···Br (15.2%), (*d*) Br···Br (5.1%), (*e*) H···H (25%) and (*f*) O···H/H···O (23.7%).

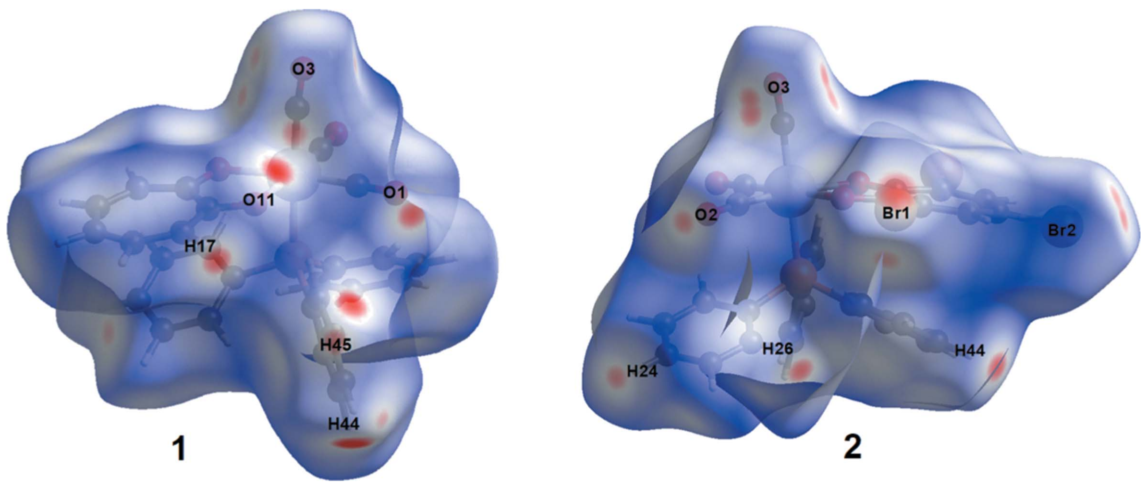

Figure 5
The Hirshfeld surfaces for **1** and **2** mapped with d_{norm} over the range from −0.2 to 1.4.

the five-membered rhenium ring system [C15—Br2···*Cg*1-($-x+1, -y+1, -z+1$) and C36—H36···O11] and atom O3 [Br2···O3($-x+1, -y+1, -z+1$) and C46—H46···O3($x+1, y, z$)] which correlates with the data given in Tables S3 and S4 in the supporting information.

Overall, the curvedness of **1** has less 'flat' regions compared to **2**, and compares well with the increased number of π-interactions observed in **2** compared to **1**.

Figs. 3 and 4 show the fingerprint plots of **1** and **2**, respectively. Fingerprint plots can be decomposed to separate the contributions from different types of interactions that overlap in the full fingerprint. In **1**, the proportion of O···H/H···O interactions comprise 28.1%, H···H comprise 38.1% and H···C/C···H comprise 26.5% of the total Hirshfeld surfaces for each molecule. In **2**, the distribution is slightly different; the C···H/H···C interactions comprise 16%, the Br···H/H···Br interactions comprise 15.2%, the Br···Br interactions comprise 5.1%, the H···H interactions comprise 25% and the O···H/H···O interactions comprise 23.7% of the total Hirshfeld surfaces.

When d_{norm} (as defined and explained by Spackman & Jayatilaka, 2009) is mapped on a Hirshfeld surface, intermolecular contacts appear as red spots, contacts shorter than van der Waal separations, on a largely blue surface. It has been proven to be useful as an unbiased method to identify close intermolecular contacts, even in complex crystal structures.

d_{norm} Hirshfeld plots of **1** and **2** are presented in Fig. 5, indicating the red spots associated with close contacts. Not all interactions are shown for conciseness because all the interactions are not visible from one orientation. All the interactions reported in Tables S1–S4 correlate with these plots.

By comparing **1** and the previously reported bis(triphenylphosphane) complex [Re(Trop)(PPh_3)$_2$(CO)$_2$] (**3**) (Gantsho *et al.*, 2020), it is clear that most of the bond lengths around the metal centre change when the axial carbonyl ligand is substituted by a second PPh_3 ligand (Table 4). When the carbonyl ligand is substituted by a PPh_3 ligand, more electron density is donated to the Re^I metal centre, shortening the equatorial Re—CO bond lengths from 1.900 (2) and 1.912 (2) Å to 1.883 (3) and 1.887 (3) Å. PPh_3 also has a weaker *trans* effect than CO, which is evident in the shortening of the Re1—P1 bond(s).

Interestingly, the *trans* effect is clearly observed in the axial Re—CO distances in the solid-state crystal structures of *fac*-[Re(Trop)(CO)$_3$(H_2O)] (Schutte *et al.*, 2012), *fac*-[Re(Trop)-

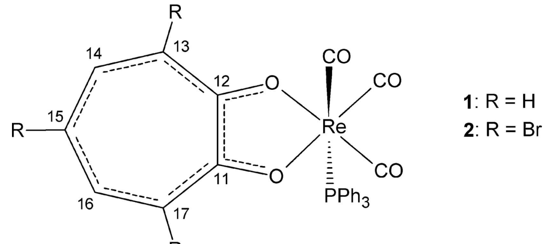

Figure 6
The atom-numbering schemes of **1** and **2**.

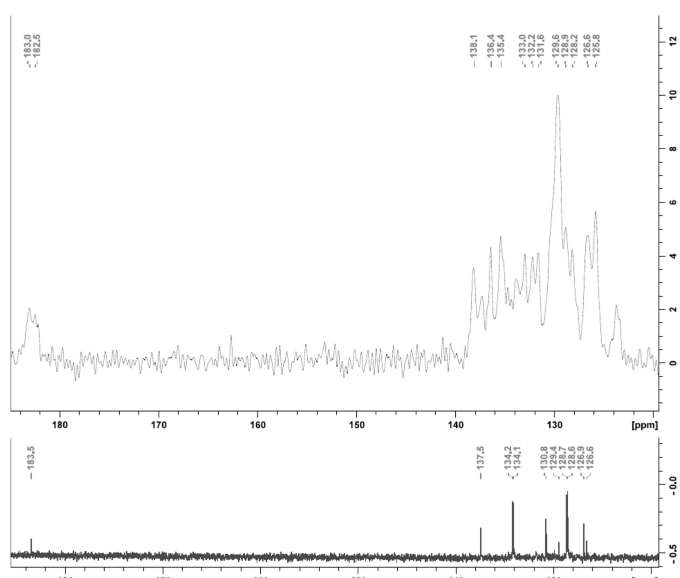

Figure 7
Solid-state *versus* liquid-state ^{13}C NMR spectra of **1**.

(Py)(CO)$_3$] (Schutte *et al.*, 2012) and *fac*-[Re(Trop)(PPh$_3$)-(CO)$_3$] [increasing from 1.890 (7) to 1.919 (4) to 1.944 (2) Å], and also in *fac*-[Re(TropBr$_3$)(CO)$_3$(H$_2$O)] (Schutte *et al.*, 2008), *fac*-[Re(TropBr$_3$)(Br)(CO)$_3$]$^-$ (Schutte *et al.*, 2007) and *fac*-[Re(TropBr$_3$)(PPh$_3$)(CO)$_3$] [increasing from 1.882 (7) to 1.897 (3) to 1.950 (5) Å] as the *trans* effect increases according to the following trend: H_2O < Py < Br < PR_3 < CO (with Py = pyridine and PR_3 = tertiary phosphane).

3.3. Solid-state NMR

In solid-state ^{13}C NMR spectroscopy, the cross polarization magic angle spinning (CP/MAS) technique is often used to enhance the polarization of the low-abundance ^{13}C nuclei *via* its interaction with ^{1}H nuclei. The effectiveness of the CP/MAS technique depends on the magnitude of ^{1}H–^{13}C dipolar coupling (Freitas *et al.*, 2016; Conte *et al.*, 2004; Smernik *et al.*, 2002). It is expected that the observed hydrogen-bond interactions, as well as other short contacts and π-interactions in the solid state, will deshield the C atoms and cause a downfield shift in the solid-state ^{13}C NMR spectra (Patterson-Elenbaum *et al.*, 2006). In the liquid state, the intra- and intermolecular interactions are disrupted because of the motion of the molecules within the solution; thus, we only observe the dynamic average of the motion. The degree of interactions present in the solid-state can be determined by the difference in chemical shift values ($\Delta\delta$) of the specific C atoms in the liquid- *versus* solid-state NMR spectra (Patterson-Elenbaum *et al.*, 2006). A larger difference in chemical shift is normally indicative of a stronger interaction, which is determined by the specific bond length and angle (Siskos *et al.*, 2017).

It is known that broad peaks (or no peaks) are observed when there are not many C atoms that are directly bound to H atoms (Freitas *et al.*, 2016), which is the case in **2**. Nevertheless, we aimed to correlate the change in chemical shift from the ^{13}C liquid-state NMR to the solid-state ^{13}C NMR to the interactions observed in the crystal structures.

Fig. 6 provides the numbering scheme of atoms in **1** and **2**. The solid-state ^{13}C NMR data of **1** did not shift much from the solution state to the solid state, with not more than a 1 ppm change ($\Delta\delta$) in the chemical shift at most, which is basically negligible (Fig. 7). Four hydrogen-bond interactions and three π-interactions are observed in **1** (Tables S1 and S2 in the supporting information), two of the π-interactions being very weak (distance > 3.8 Å). The five interactions that are considered to be stronger with shorter distances involve the PPh$_3$ ligand, the O atoms of the tropolonate ligand, the carbonyl ligands and the centroid of the five-membered Re1/O11/C11/C12/O12 ring system. The carbonyl ligands are not visible on the liquid- and solid-state ^{13}C NMR spectra due to the economic and time implications involved to observe it. IR spectroscopy are used to confirm the presence of the carbonyl ligands in this type of complex.

In the solution-state ^{13}C NMR spectra, the peak at 184 ppm is assigned to C11 and C12, and seeing that these atoms are bound to O11 and O12 (involved in three interactions) and are part of the five-membered ring system (Re1/O11/C11/C12/O12), a downfield shift is expected because of the effect of the

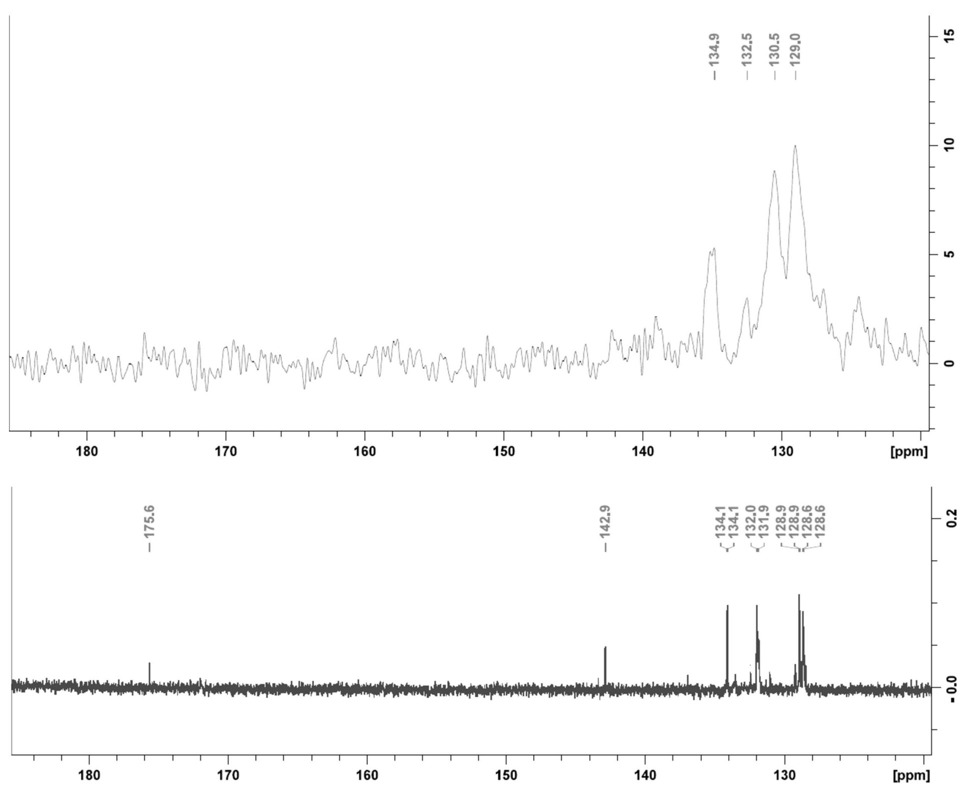

Figure 8
Solution-state *versus* solid-state ^{13}C NMR spectra of **2**.

deshielding of these interactions. However, it shifted slightly upfield to 183 and 182 ppm, and yielded two peaks in the solid state compared to a single peak in the solution state. This is due to the fact that C11 and C12 are not equivalent in the solid state because of the interactions observed in the crystal structure: C17—H17···O1($-x+2$, $-y+1$, $-z$), C45—H45···O11($-x+2$, $-y+1$, $-z$) and C46—H46···O11 all indirectly involve C11, while C44—H44···O12(x, $y+1$, z) is the only interaction that indirectly involves C12; thus, the splitting of the single peak in the solid state.

The single peak for C13, C14, C16 and C17 at 138 ppm, the peaks for the PPh_3 ligand at 134, 131 and 129 ppm, and the single peak for C15 at 127 ppm in the solution state are not as well defined in the solid state and yield a broad peak from 138 to 126 ppm, similar to the range found in the solution state; we expected a downfield shift because of the interactions involving the tropolonate ring system and one arene ring of the PPh_3 ligand. We could, however, see some significant splitting of the peaks; compared to the five single peaks at 138, 134, 131, 129 and 127 ppm in the solution state, splitting of the peaks (although it is a broad peak) is seen in the solid state, indicating that many of the C atoms are not equivalent anymore because of the interactions observed in the crystal structure [C17—H17···O1($-x+2$, $-y+1$, $-z$), meaning C13, C14, C16 and C17 are not equivalent anymore; C44—H44···O12(x, $y+1$, z), C45—H45···O11($-x+2$, $-y+1$, $-z$) and C46—H46···O11, meaning the C41–C46 arene ring in PPh_3 is not equivalent to the C21–C26 and C31–C36 arene rings].

In the case of **2**, the fact that the tribromotropolonate ring system only has two H atoms directly bound to C atoms had an impact on the solid-state ^{13}C NMR spectra and we only observe the PPh_3 ligand, and the seven C atoms in the tribromotropolonate ligand are not observed (Fig. 8) (Freitas *et al.*, 2016). In the solution-state spectra, the PPh_3 ligand has a single peak at 134 ppm which split up into four peaks at 135, 132, 131 and 129 ppm in the solid-state spectra. Again, this is because the C atoms are not equivalent in the solid state.

4. Conclusion

Two new crystal structures of rhenium(I) tricarbonyl complexes with either a tropolonate or a tribromotropolonate bidentate ligand are reported and correspond well with similar known structures. The solid-state NMR data indicated the presence of inter- and intramolecular interactions, as seen by the splitting of some signals, but unfortunately, due to the fact that both **1** and **2** contain only a few C—H units each, credible chemical shifts could not be obtained and correlated with the crystal data. The intermolecular interactions obtained from *PLATON* (Spek, 2020) correlate with the Hirshfeld surfaces generated with *CrystalExplorer* (Spackman *et al.*, 2021).

Acknowledgements

Christo van Staden and Francois Jacobs are gratefully acknowledged for the data collection for the crystal structures. This work is based on research supported in part by the National Research Foundation of South Africa. The grant holder acknowledges that opinions, findings and conclusions or recommendations expressed in any publication generated by NRF supported research are that of the author(s) and that the NRF accepts no liability whatsoever in this regard.

Funding information

Funding for this research was provided by: National Research Foundation (grant No. 116246).

References

Bochkova, R. I., Zakharov, L. N., Patrikeeva, N. V., Shal'nova, K. G., Abakumov, G. A. & Cherkasov, V. K. (1987). *Koord. Khim.* **13**, 702.
Borowski, P., Lang, M., Haag, A. & Baier, A. (2007). *Antivir. Chem. Chemother.* **18**, 103–109.
Brandenburg, K. & Putz, H. (2019). *DIAMOND*. Crystal Impact GbR, Bonn, Germany.
Brink, A., Kroon, R. E., Visser, H. G., van Rensburg, C. E. J. & Roodt, A. (2018). *New J. Chem.* **42**, 5193–5203.
Bruker (2012). *APEX2*, *SAINT* and *SADABS*. Bruker AXS Inc., Madison, Wisconsin, USA.
Chierotti, M. R. & Gobetto, R. (2008). *Chem. Commun.* pp. 1621–1634.
Collery, P., Desmaele, D. & Vijaykumar, V. (2019). *Curr. Pharm. Des.* **25**, 3306–3322.
Conte, P., Spaccini, R. & Piccolo, A. (2004). *Prog. Nucl. Magn. Reson. Spectrosc.* **44**, 215–223.
Dittes, U., Diemer, R. & Keppler, B. K. (1995*a*). *J. Cancer Res. Clin. Oncol.* **121**, A50.
Dittes, U., Diemer, R., Lenz, O. & Keppler, B. K. (1995*b*). *J. Inorg. Biochem.* **59**, 215.
Farrugia, L. J. (2012). *J. Appl. Cryst.* **45**, 849–854.
Freitas, J. C. C., Cipriano, D. F., Zucolotto, C. G., Cunha, A. G. & Emmerich, F. G. (2016). *J. Spectrosc.* **2016**, 1543273.
Gantsho, V. L., Dotou, M., Jakubaszek, M., Goud, B., Gasser, G., Visser, H. G. & Schutte-Smith, M. (2020). *Dalton Trans.* **49**, 35–46.
Ishihara, M., Wakabayashi, H., Motohashi, N. & Sakagami, H. (2010). *Anticancer Res.* **30**, 129–133.
Kydonaki, T. E., Tsoukas, E., Mendes, F., Hatzidimitriou, A. G., Paulo, A., Papadopoulou, L. C., Papagiannopoulou, D. & Psomas, G. (2016). *J. Inorg. Biochem.* **160**, 94–105.
Leonidova, A. & Gasser, G. (2014). *ACS Chem. Biol.* 9, 2180–2193.
Li, M., Liu, X., Nie, M., Wu, Z., Yi, C., Chen, G. & Yam, V. W. (2012). *Organometallics*, **31**, 4459–4466.
Manicum, A.-L., Alexander, O., Schutte-Smith, M. & Visser, H. G. (2020). *J. Mol. Struct.* **1209**, 127953.
Otero, C., Carreño, A., Polanco, R., Llancalahuen, F. M., Arratia-Pérez, R., Gacitúa, M. & Fuentes, J. A. (2019). *Front. Chem.* **7**, 454.
Patterson-Elenbaum, S., Stanley, J. T., Dillner, D. K., Lin, S. & Traficante, D. (2006). *Magn. Reson. Chem.* **44**, 797–806.
Schutte, M., Kemp, G., Visser, H. G. & Roodt, A. (2011). *Inorg. Chem.* **50**, 12486–12498.
Schutte, M., Roodt, A. & Visser, H. G. (2012). *Inorg. Chem.* **51**, 11996–12006.
Schutte, M., Visser, H. G. & Roodt, A. (2008). *Acta Cryst.* E**64**, m1610–m1611.
Schutte, M., Visser, H. G. & Steyl, G. (2007). *Acta Cryst.* E**63**, m3195–m3196.
Schutte-Smith, M., Marker, S. C., Wilson, J. J. & Visser, H. G. (2020). *Inorg. Chem.* **59**, 15888–15897.
Schutte-Smith, M., Roodt, A., Alberto, R., Twigge, L., Visser, H. G., Kirsten, L. & Koen, R. (2019*a*). *Acta Cryst.* C**75**, 378–387.
Schutte-Smith, M., Roodt, A. & Visser, H. G. (2019*b*). *Dalton Trans.* **48**, 9984–9997.

Schutte-Smith, M. & Visser, H. G. (2015). *Polyhedron*, **89**, 122–128.
Seth, S. K., Mandal, P. C., Kar, T. & Mukhopadhyay, S. (2011). *J. Mol. Struct.* **994**, 109–116.
Sheldrick, G. M. (2015*a*). *Acta Cryst.* A**71**, 3–8.
Sheldrick, G. M. (2015*b*). *Acta Cryst.* C**71**, 3–8.
Siskos, M. G., Choudhary, M. I. & Gerothanassis, I. P. (2017). *Molecules*, **22**, 415.
Smernik, R. J., Baldock, J. A. & Oades, J. M. (2002). *Solid State Nucl. Magn. Reson.* **22**, 71–82.
Sovari, S. N., Radakovic, N., Roch, P., Crochet, A., Pavic, A. & Zobi, F. (2021). *Eur. J. Med. Chem.* **226**, 113858.
Sovari, S. N., Vojnovic, S., Bogojevic, S. S., Crochet, A., Pavic, A., Nikodinovic-Runic, J. & Zobi, F. (2020). *Eur. J. Med. Chem.* **205**, 112533.
Spackman, M. A. & Jayatilaka, D. (2009). *CrystEngComm*, **11**, 19–32.
Spackman, P. R., Turner, M. J., McKinnon, J. J., Wolff, S. K. & Spackman, M. A. (2021). *CrystalExplorer*. Version 21.5. University of Western Australia. https://crystalexplorer.scb.uwa.edu.au/.
Spek, A. L. (2020). *Acta Cryst.* E**76**, 1–11.
Traer, J. W., Britten, J. F. & Goward, G. R. (2007). *J. Phys. Chem. B*, **111**, 5602–5609.
Trust, T. J. (1975). *Antimicrob. Agents Chemother.* **7**, 500–506.
Varma, R. R., Pursuwani, B. H., Suresh, E., Bhatt, B. S. & Patel, M. N. (2020). *J. Mol. Struct.* **1200**, 127068.
Wilhelm, A., Bonnet, S., Twigge, L., Rarova, L., Stenclova, T., Visser, H. G. & Schutte-Smith, M. (2022). *J. Mol. Struct.* **1251**, 132001.
Zhao, X., Edén, M. & Levitt, M. A. (2001). *Chem. Phys. Lett.* **342**, 353–361.

supporting information

Acta Cryst. (2022). C**78**, 351-359 [https://doi.org/10.1107/S205322962200465X]

Crystal and molecular structures of *fac*-[Re(Bid)(PPh_3)$(CO)_3$] [Bid is tropolone (TropH) and tribromotropolone ($TropBr_3H$)]

Marietjie Schutte-Smith and Hendrik Gideon Visser

Computing details

For both structures, data collection: *APEX2* (Bruker, 2012); cell refinement: *SAINT-Plus* (Bruker, 2012); data reduction: *SAINT-Plus* (Bruker, 2012); program(s) used to solve structure: SHELXT (Sheldrick, 2015*a*); program(s) used to refine structure: *SHELXL2018* (Sheldrick, 2015*b*); molecular graphics: *DIAMOND* (Brandenburg & Putz, 2019); software used to prepare material for publication: *WinGX* (Farrugia, 2012) and *DIAMOND* (Brandenburg & Putz, 2019).

fac-Tricarbonyl(triphenylphosphane-*κP*)(tropolonato-κ^2O,O')rhenium(I) (1)

Crystal data

[Re($C_7H_5O_2$)($C_{18}H_{15}P$)$(CO)_3$]
M_r = 653.61
Triclinic, $P\overline{1}$
a = 9.9301 (11) Å
b = 10.1686 (10) Å
c = 12.7882 (14) Å
α = 80.948 (3)°
β = 71.899 (3)°
γ = 88.682 (3)°
V = 1211.6 (2) Å^3
Z = 2
$F(000)$ = 636
D_x = 1.792 Mg m^{-3}
Mo $K\alpha$ radiation, λ = 0.71073 Å
Cell parameters from 9782 reflections
θ = 2.9–28.3°
μ = 5.12 mm^{-1}
T = 100 K
Cuboid, orange
0.27 × 0.17 × 0.13 mm

Data collection

Bruker APEXII CCD diffractometer
φ and ω scans
Absorption correction: multi-scan (SADABS; Bruker, 2012)
T_{min} = 0.357, T_{max} = 0.511
25538 measured reflections
5820 independent reflections
5726 reflections with $I > 2\sigma(I)$
R_{int} = 0.037
θ_{max} = 28.0°, θ_{min} = 2.9°
h = −13→13
k = −13→13
l = −16→16

Refinement

Refinement on F^2
Least-squares matrix: full
$R[F^2 > 2\sigma(F^2)]$ = 0.015
$wR(F^2)$ = 0.038
S = 1.08
5820 reflections
316 parameters
0 restraints
Hydrogen site location: inferred from neighbouring sites
H-atom parameters constrained
$w = 1/[\sigma^2(F_o^2) + 0.7798P]$ where $P = (F_o^2 + 2F_c^2)/3$
$(\Delta/\sigma)_{max}$ = 0.003
$\Delta\rho_{max}$ = 0.46 e Å^{-3}
$\Delta\rho_{min}$ = −0.60 e Å^{-3}

Special details

Geometry. All esds (except the esd in the dihedral angle between two l.s. planes) are estimated using the full covariance matrix. The cell esds are taken into account individually in the estimation of esds in distances, angles and torsion angles; correlations between esds in cell parameters are only used when they are defined by crystal symmetry. An approximate (isotropic) treatment of cell esds is used for estimating esds involving l.s. planes.

Refinement. The reflection data of *fac*-[Re(Trop)(PPh_3)($CO)_3$] and *fac*-[Re(TropBr$_3$)(PPh_3)($CO)_3$] were collected at 100 (2) K on a Bruker D8 Quest Eco Chi Photon II CPAD diffractometer using Mo *Kα* radiation (λ = 0.71073 Å) and at 104 (2) K on a Bruker D8 Venture 4K Kappa Photon III C28 diffractometer also using Mo *Kα* radiation (λ = 0.71073 Å), respectively. The unit-cell parameters were refined by *SAINT-Plus* (Bruker, 2012), while *SADABS* (Bruker, 2012) was used for absorption corrections. The structures were solved by direct methods and refined on F^2 using anisotropic displacement parameters for all non-H atoms. *SHELXL97* (Sheldrick, 1997, 2008) and *WinGX* (Farrugia, 2012) were used for structure solutions and refinements, respectively. The molecular graphics were prepared with *DIAMOND* (Brandenburg & Putz, 2019).

Fractional atomic coordinates and isotropic or equivalent isotropic displacement parameters (Å^2)

	x	*y*	*z*	U_{iso}*/U_{eq}
Re1	0.90667 (2)	0.18057 (2)	0.20344 (2)	0.01253 (3)
P1	0.75009 (5)	0.32233 (5)	0.33175 (4)	0.01302 (9)
O12	0.72021 (14)	0.08360 (13)	0.20023 (11)	0.0173 (3)
O11	0.84257 (15)	0.29691 (14)	0.07383 (11)	0.0185 (3)
O2	0.95372 (19)	−0.00475 (16)	0.40161 (13)	0.0331 (4)
O3	1.11659 (16)	0.00229 (16)	0.05887 (13)	0.0266 (3)
C2	0.9374 (2)	0.0666 (2)	0.32747 (17)	0.0201 (4)
O1	1.16119 (16)	0.36066 (16)	0.17730 (13)	0.0281 (3)
C3	1.0340 (2)	0.06850 (19)	0.10871 (16)	0.0182 (4)
C1	1.0657 (2)	0.2900 (2)	0.18974 (16)	0.0185 (4)
C21	0.56224 (19)	0.28800 (18)	0.35765 (15)	0.0149 (3)
C11	0.7241 (2)	0.2633 (2)	0.06194 (16)	0.0195 (4)
C12	0.6555 (2)	0.1414 (2)	0.13322 (16)	0.0187 (4)
C22	0.4701 (2)	0.3853 (2)	0.33403 (16)	0.0196 (4)
H22	0.503393	0.474971	0.307256	0.024*
C41	0.77452 (19)	0.50141 (18)	0.28609 (15)	0.0152 (3)
C46	0.8520 (2)	0.5519 (2)	0.17672 (17)	0.0221 (4)
H46	0.893136	0.492594	0.125721	0.027*
C23	0.3293 (2)	0.3515 (2)	0.34958 (18)	0.0250 (4)
H23	0.266556	0.418322	0.334279	0.030*
C31	0.7728 (2)	0.30410 (18)	0.46994 (15)	0.0159 (3)
C24	0.2805 (2)	0.2210 (2)	0.38720 (17)	0.0242 (4)
H24	0.184702	0.198099	0.396922	0.029*
C26	0.5115 (2)	0.15676 (19)	0.39609 (15)	0.0180 (4)
H26	0.573467	0.089675	0.412313	0.022*
C25	0.3717 (2)	0.1234 (2)	0.41080 (17)	0.0211 (4)
H25	0.338152	0.033770	0.437030	0.025*
C44	0.8087 (2)	0.7755 (2)	0.21524 (19)	0.0251 (4)
H44	0.818632	0.868908	0.190649	0.030*
C15	0.4437 (3)	0.2377 (3)	−0.0044 (2)	0.0457 (7)
H15	0.367881	0.248628	−0.035242	0.055*
C43	0.7332 (2)	0.7260 (2)	0.32494 (18)	0.0229 (4)

H43	0.692734	0.785739	0.375718	0.027*
C45	0.8693 (2)	0.6886 (2)	0.14175 (18)	0.0276 (5)
H45	0.923081	0.722490	0.067145	0.033*
C42	0.7166 (2)	0.58972 (19)	0.36065 (16)	0.0196 (4)
H42	0.665658	0.556270	0.436029	0.024*
C13	0.5279 (2)	0.0836 (2)	0.13450 (19)	0.0292 (5)
H13	0.500094	0.002253	0.184346	0.035*
C32	0.9066 (2)	0.3319 (2)	0.47581 (18)	0.0243 (4)
H32	0.982195	0.358266	0.409087	0.029*
C34	0.8210 (3)	0.2831 (2)	0.67566 (18)	0.0308 (5)
H34	0.837615	0.274798	0.745648	0.037*
C36	0.6628 (2)	0.2668 (2)	0.56869 (16)	0.0226 (4)
H36	0.570583	0.248217	0.566301	0.027*
C35	0.6880 (3)	0.2567 (2)	0.67093 (17)	0.0300 (5)
H35	0.612589	0.231408	0.737966	0.036*
C14	0.4359 (3)	0.1264 (3)	0.0746 (2)	0.0410 (6)
H14	0.354599	0.070191	0.090460	0.049*
C17	0.6736 (3)	0.3459 (2)	−0.01570 (18)	0.0299 (5)
H17	0.733164	0.420839	−0.055596	0.036*
C33	0.9310 (2)	0.3217 (2)	0.57793 (19)	0.0298 (5)
H33	1.022738	0.341205	0.580892	0.036*
C16	0.5500 (3)	0.3350 (3)	−0.0433 (2)	0.0406 (6)
H16	0.536517	0.405252	−0.097247	0.049*

Atomic displacement parameters (Å^2)

	U^{11}	U^{22}	U^{33}	U^{12}	U^{13}	U^{23}
Re1	0.01235 (4)	0.01212 (4)	0.01298 (4)	0.00146 (3)	−0.00321 (3)	−0.00325 (3)
P1	0.0130 (2)	0.0131 (2)	0.0120 (2)	0.00118 (16)	−0.00242 (17)	−0.00256 (16)
O12	0.0152 (6)	0.0153 (6)	0.0218 (7)	0.0003 (5)	−0.0050 (5)	−0.0055 (5)
O11	0.0215 (7)	0.0178 (7)	0.0165 (6)	0.0016 (5)	−0.0067 (5)	−0.0019 (5)
O2	0.0441 (10)	0.0296 (9)	0.0276 (8)	0.0072 (7)	−0.0174 (7)	0.0020 (6)
O3	0.0206 (7)	0.0297 (8)	0.0321 (8)	0.0082 (6)	−0.0063 (6)	−0.0176 (7)
C2	0.0190 (9)	0.0188 (9)	0.0227 (10)	0.0024 (7)	−0.0059 (8)	−0.0058 (7)
O1	0.0219 (7)	0.0300 (8)	0.0325 (8)	−0.0079 (6)	−0.0079 (6)	−0.0050 (6)
C3	0.0185 (9)	0.0177 (9)	0.0203 (9)	−0.0001 (7)	−0.0076 (7)	−0.0050 (7)
C1	0.0191 (9)	0.0189 (9)	0.0165 (9)	0.0026 (7)	−0.0033 (7)	−0.0047 (7)
C21	0.0143 (8)	0.0173 (9)	0.0130 (8)	0.0012 (7)	−0.0032 (7)	−0.0039 (6)
C11	0.0202 (9)	0.0240 (10)	0.0175 (9)	0.0082 (8)	−0.0073 (7)	−0.0111 (7)
C12	0.0174 (9)	0.0215 (9)	0.0204 (9)	0.0061 (7)	−0.0061 (7)	−0.0129 (7)
C22	0.0205 (9)	0.0180 (9)	0.0222 (9)	0.0013 (7)	−0.0085 (8)	−0.0047 (7)
C41	0.0148 (8)	0.0125 (8)	0.0184 (9)	0.0003 (6)	−0.0052 (7)	−0.0029 (6)
C46	0.0266 (10)	0.0167 (9)	0.0206 (9)	0.0046 (8)	−0.0028 (8)	−0.0053 (7)
C23	0.0200 (10)	0.0263 (11)	0.0328 (11)	0.0062 (8)	−0.0131 (9)	−0.0077 (8)
C31	0.0186 (9)	0.0154 (8)	0.0142 (8)	0.0036 (7)	−0.0054 (7)	−0.0035 (6)
C24	0.0154 (9)	0.0322 (11)	0.0264 (10)	−0.0004 (8)	−0.0068 (8)	−0.0080 (8)
C26	0.0179 (9)	0.0195 (9)	0.0152 (8)	0.0012 (7)	−0.0035 (7)	−0.0020 (7)
C25	0.0203 (10)	0.0220 (10)	0.0194 (9)	−0.0035 (8)	−0.0040 (8)	−0.0026 (7)

C44	0.0259 (10)	0.0128 (9)	0.0342 (11)	−0.0003 (8)	−0.0062 (9)	−0.0031 (8)
C15	0.0330 (13)	0.079 (2)	0.0416 (15)	0.0235 (14)	−0.0252 (12)	−0.0320 (15)
C43	0.0214 (9)	0.0176 (9)	0.0306 (11)	0.0029 (7)	−0.0055 (8)	−0.0120 (8)
C45	0.0325 (11)	0.0169 (10)	0.0235 (10)	0.0014 (8)	0.0032 (9)	0.0015 (8)
C42	0.0206 (9)	0.0186 (9)	0.0185 (9)	0.0017 (7)	−0.0028 (7)	−0.0066 (7)
C13	0.0203 (10)	0.0375 (13)	0.0336 (12)	−0.0001 (9)	−0.0076 (9)	−0.0182 (10)
C32	0.0186 (9)	0.0343 (12)	0.0212 (10)	0.0051 (8)	−0.0066 (8)	−0.0080 (8)
C34	0.0470 (14)	0.0296 (12)	0.0222 (10)	0.0077 (10)	−0.0191 (10)	−0.0069 (8)
C36	0.0243 (10)	0.0240 (10)	0.0175 (9)	−0.0036 (8)	−0.0029 (8)	−0.0045 (7)
C35	0.0425 (13)	0.0304 (12)	0.0143 (9)	−0.0047 (10)	−0.0055 (9)	−0.0019 (8)
C14	0.0220 (11)	0.0669 (19)	0.0447 (15)	0.0060 (11)	−0.0151 (11)	−0.0310 (13)
C17	0.0371 (12)	0.0344 (12)	0.0222 (10)	0.0126 (10)	−0.0142 (9)	−0.0078 (9)
C33	0.0277 (11)	0.0392 (13)	0.0299 (11)	0.0082 (9)	−0.0163 (9)	−0.0127 (9)
C16	0.0462 (15)	0.0579 (17)	0.0298 (12)	0.0290 (13)	−0.0248 (11)	−0.0200 (11)

Geometric parameters (Å, º)

Re1—C1	1.900 (2)	C24—H24	0.9500
Re1—C2	1.912 (2)	C26—C25	1.384 (3)
Re1—C3	1.944 (2)	C26—H26	0.9500
Re1—O12	2.1322 (13)	C25—H25	0.9500
Re1—O11	2.1345 (13)	C44—C45	1.383 (3)
Re1—P1	2.4987 (5)	C44—C43	1.387 (3)
P1—C41	1.8203 (19)	C44—H44	0.9500
P1—C21	1.8224 (19)	C15—C14	1.379 (4)
P1—C31	1.8305 (18)	C15—C16	1.380 (4)
O12—C12	1.288 (2)	C15—H15	0.9500
O11—C11	1.293 (2)	C43—C42	1.386 (3)
O2—C2	1.151 (3)	C43—H43	0.9500
O3—C3	1.148 (2)	C45—H45	0.9500
O1—C1	1.159 (2)	C42—H42	0.9500
C21—C22	1.395 (3)	C13—C14	1.386 (3)
C21—C26	1.395 (3)	C13—H13	0.9500
C11—C17	1.403 (3)	C32—C33	1.388 (3)
C11—C12	1.459 (3)	C32—H32	0.9500
C12—C13	1.404 (3)	C34—C35	1.375 (3)
C22—C23	1.393 (3)	C34—C33	1.388 (3)
C22—H22	0.9500	C34—H34	0.9500
C41—C46	1.391 (3)	C36—C35	1.394 (3)
C41—C42	1.397 (3)	C36—H36	0.9500
C46—C45	1.389 (3)	C35—H35	0.9500
C46—H46	0.9500	C14—H14	0.9500
C23—C24	1.382 (3)	C17—C16	1.390 (3)
C23—H23	0.9500	C17—H17	0.9500
C31—C32	1.392 (3)	C33—H33	0.9500
C31—C36	1.394 (3)	C16—H16	0.9500
C24—C25	1.390 (3)		

C1—Re1—C2	90.76 (8)	C23—C24—H24	120.0
C1—Re1—C3	88.64 (8)	C25—C24—H24	120.0
C2—Re1—C3	87.11 (8)	C25—C26—C21	120.62 (18)
C1—Re1—O12	170.57 (7)	C25—C26—H26	119.7
C2—Re1—O12	98.46 (7)	C21—C26—H26	119.7
C3—Re1—O12	93.75 (7)	C26—C25—C24	119.99 (19)
C1—Re1—O11	96.70 (7)	C26—C25—H25	120.0
C2—Re1—O11	171.97 (7)	C24—C25—H25	120.0
C3—Re1—O11	96.00 (7)	C45—C44—C43	119.92 (19)
O12—Re1—O11	73.99 (5)	C45—C44—H44	120.0
C1—Re1—P1	89.87 (6)	C43—C44—H44	120.0
C2—Re1—P1	90.48 (6)	C14—C15—C16	126.9 (2)
C3—Re1—P1	177.15 (6)	C14—C15—H15	116.5
O12—Re1—P1	88.10 (4)	C16—C15—H15	116.5
O11—Re1—P1	86.59 (4)	C42—C43—C44	120.18 (18)
C41—P1—C21	105.23 (8)	C42—C43—H43	119.9
C41—P1—C31	101.97 (8)	C44—C43—H43	119.9
C21—P1—C31	105.15 (8)	C44—C45—C46	120.18 (19)
C41—P1—Re1	115.75 (6)	C44—C45—H45	119.9
C21—P1—Re1	112.81 (6)	C46—C45—H45	119.9
C31—P1—Re1	114.69 (6)	C43—C42—C41	120.18 (18)
C12—O12—Re1	117.43 (12)	C43—C42—H42	119.9
C11—O11—Re1	117.33 (12)	C41—C42—H42	119.9
O2—C2—Re1	178.07 (18)	C14—C13—C12	130.3 (2)
O3—C3—Re1	173.87 (17)	C14—C13—H13	114.9
O1—C1—Re1	176.74 (18)	C12—C13—H13	114.9
C22—C21—C26	119.03 (17)	C33—C32—C31	120.8 (2)
C22—C21—P1	122.77 (14)	C33—C32—H32	119.6
C26—C21—P1	118.07 (14)	C31—C32—H32	119.6
O11—C11—C17	118.1 (2)	C35—C34—C33	119.8 (2)
O11—C11—C12	115.25 (17)	C35—C34—H34	120.1
C17—C11—C12	126.62 (19)	C33—C34—H34	120.1
O12—C12—C13	118.46 (19)	C35—C36—C31	120.1 (2)
O12—C12—C11	115.62 (16)	C35—C36—H36	120.0
C13—C12—C11	125.92 (19)	C31—C36—H36	120.0
C23—C22—C21	120.16 (18)	C34—C35—C36	120.6 (2)
C23—C22—H22	119.9	C34—C35—H35	119.7
C21—C22—H22	119.9	C36—C35—H35	119.7
C46—C41—C42	119.24 (17)	C15—C14—C13	130.2 (3)
C46—C41—P1	120.36 (14)	C15—C14—H14	114.9
C42—C41—P1	120.40 (14)	C13—C14—H14	114.9
C45—C46—C41	120.27 (18)	C16—C17—C11	130.0 (2)
C45—C46—H46	119.9	C16—C17—H17	115.0
C41—C46—H46	119.9	C11—C17—H17	115.0
C24—C23—C22	120.24 (19)	C34—C33—C32	119.8 (2)
C24—C23—H23	119.9	C34—C33—H33	120.1
C22—C23—H23	119.9	C32—C33—H33	120.1
C32—C31—C36	118.81 (18)	C15—C16—C17	129.9 (3)

C32—C31—P1	117.76 (15)	C15—C16—H16	115.0
C36—C31—P1	123.42 (15)	C17—C16—H16	115.0
C23—C24—C25	119.95 (18)		

Hydrogen-bond geometry (Å, º)

D—H···*A*	*D*—H	H···*A*	*D*···*A*	*D*—H···*A*
C17—H17···O1[i]	0.95	2.54	3.471 (3)	166
C44—H44···O12[ii]	0.95	2.38	3.227 (2)	149
C45—H45···O11[i]	0.95	2.49	3.286 (3)	142
C46—H46···O11	0.95	2.31	3.102 (2)	141

Symmetry codes: (i) $-x+2, -y+1, -z$; (ii) $x, y+1, z$.

fac-Tricarbonyl(3,5,7-tribromotropolonato-κ^2O,O')(triphenylphosphane-κP)rhenium(I) (2)

Crystal data

$[Re(C_7H_2Br_3O_2)(C_{18}H_{15}P)(CO)_3]$
M_r = 890.32
Triclinic, $P\overline{1}$
a = 8.5413 (12) Å
b = 8.7024 (13) Å
c = 20.376 (3) Å
α = 102.221 (5)°
β = 93.891 (5)°
γ = 109.093 (5)°
V = 1383.3 (3) Å^3
Z = 2
$F(000)$ = 840
D_x = 2.138 Mg m^{-3}
Mo $K\alpha$ radiation, λ = 0.71073 Å
Cell parameters from 9973 reflections
θ = 2.6–28.3°
μ = 8.82 mm^{-1}
T = 104 K
Stout, orange
0.18 × 0.04 × 0.04 mm

Data collection

Bruker APEXII CCD diffractometer
φ and ω scans
Absorption correction: multi-scan (SADABS; Bruker, 2012)
T_{min} = 0.690, T_{max} = 0.728
34880 measured reflections
6818 independent reflections
5913 reflections with $I > 2\sigma(I)$
R_{int} = 0.068
θ_{max} = 28.3°, θ_{min} = 2.1°
h = −11→11
k = −11→11
l = −27→27

Refinement

Refinement on F^2
Least-squares matrix: full
$R[F^2 > 2\sigma(F^2)]$ = 0.029
$wR(F^2)$ = 0.062
S = 1.06
6818 reflections
343 parameters
0 restraints
Hydrogen site location: inferred from neighbouring sites
H-atom parameters constrained
$w = 1/[\sigma^2(F_o^2) + 2.6793P]$ where $P = (F_o^2 + 2F_c^2)/3$
$(\Delta/\sigma)_{max}$ = 0.001
$\Delta\rho_{max}$ = 0.93 e Å^{-3}
$\Delta\rho_{min}$ = −1.48 e Å^{-3}

Special details

Geometry. All esds (except the esd in the dihedral angle between two l.s. planes) are estimated using the full covariance matrix. The cell esds are taken into account individually in the estimation of esds in distances, angles and torsion angles; correlations between esds in cell parameters are only used when they are defined by crystal symmetry. An approximate (isotropic) treatment of cell esds is used for estimating esds involving l.s. planes.

Fractional atomic coordinates and isotropic or equivalent isotropic displacement parameters ($Å^2$)

	x	*y*	*z*	U_{iso}*/U_{eq}
Re1	0.34371 (2)	0.51462 (2)	0.23619 (2)	0.01495 (5)
Br1	0.20138 (5)	0.09101 (5)	0.37277 (2)	0.02757 (11)
Br3	0.84257 (5)	0.83501 (6)	0.41990 (2)	0.02938 (11)
Br2	0.78047 (5)	0.33967 (6)	0.54936 (2)	0.03099 (11)
P1	0.54024 (11)	0.39220 (13)	0.18066 (5)	0.0151 (2)
O12	0.3101 (3)	0.3526 (3)	0.30298 (14)	0.0173 (6)
O11	0.5457 (3)	0.6347 (3)	0.32020 (13)	0.0168 (6)
O1	0.4042 (4)	0.7481 (4)	0.14031 (15)	0.0252 (7)
O2	0.0536 (3)	0.2717 (4)	0.12850 (16)	0.0286 (7)
O3	0.1118 (4)	0.6938 (4)	0.29969 (16)	0.0263 (7)
C1	0.3838 (4)	0.6630 (5)	0.1768 (2)	0.0166 (8)
C31	0.7272 (4)	0.5482 (5)	0.1641 (2)	0.0177 (8)
C12	0.4222 (5)	0.3904 (5)	0.3542 (2)	0.0171 (8)
C16	0.7463 (5)	0.5456 (5)	0.4653 (2)	0.0207 (9)
H16	0.850648	0.611307	0.493127	0.025*
C13	0.4042 (5)	0.2776 (5)	0.3969 (2)	0.0192 (8)
C11	0.5588 (4)	0.5511 (5)	0.36368 (19)	0.0155 (7)
C14	0.5107 (5)	0.2750 (5)	0.4502 (2)	0.0207 (8)
H14	0.473096	0.180912	0.469142	0.025*
C2	0.1619 (5)	0.3673 (5)	0.1684 (2)	0.0196 (8)
C15	0.6653 (5)	0.3928 (6)	0.4791 (2)	0.0216 (9)
C36	0.7773 (5)	0.7145 (5)	0.1999 (2)	0.0195 (8)
H36	0.713497	0.747856	0.232854	0.023*
C3	0.1976 (5)	0.6252 (5)	0.2784 (2)	0.0195 (8)
C41	0.6223 (5)	0.2739 (5)	0.22865 (19)	0.0164 (8)
C17	0.6966 (5)	0.6162 (5)	0.4167 (2)	0.0188 (8)
C21	0.4454 (5)	0.2534 (5)	0.0969 (2)	0.0182 (8)
C35	0.9204 (5)	0.8337 (6)	0.1882 (2)	0.0248 (9)
H35	0.953631	0.948010	0.212415	0.030*
C33	0.9654 (5)	0.6163 (6)	0.1050 (2)	0.0271 (10)
H33	1.030558	0.582921	0.072702	0.033*
C32	0.8217 (5)	0.4985 (5)	0.1167 (2)	0.0212 (8)
H32	0.788150	0.384355	0.092208	0.025*
C42	0.5127 (5)	0.1357 (5)	0.2467 (2)	0.0209 (8)
H42	0.395756	0.099066	0.231562	0.025*
C34	1.0131 (5)	0.7830 (6)	0.1408 (2)	0.0252 (10)
H34	1.110932	0.863403	0.132541	0.030*
C26	0.3990 (5)	0.0804 (5)	0.0832 (2)	0.0254 (9)
H26	0.427315	0.029290	0.116835	0.031*
C22	0.4046 (5)	0.3266 (5)	0.0467 (2)	0.0231 (9)
H22	0.435001	0.445147	0.055876	0.028*
C45	0.8523 (6)	0.2426 (7)	0.2927 (3)	0.0348 (11)
H45	0.968798	0.279725	0.308745	0.042*
C43	0.5751 (6)	0.0525 (5)	0.2867 (2)	0.0261 (9)
H43	0.500716	−0.042640	0.298282	0.031*

C23	0.3206 (5)	0.2281 (6)	−0.0159 (2)	0.0290 (10)
H23	0.296538	0.278796	−0.050383	0.035*
C24	0.2706 (6)	0.0541 (7)	−0.0289 (2)	0.0345 (12)
H24	0.208942	−0.014516	−0.071564	0.041*
C46	0.7922 (5)	0.3259 (6)	0.2522 (2)	0.0250 (9)
H46	0.868070	0.419631	0.240333	0.030*
C44	0.7445 (6)	0.1066 (6)	0.3100 (2)	0.0305 (10)
H44	0.786296	0.049770	0.337883	0.037*
C25	0.3114 (6)	−0.0175 (6)	0.0206 (2)	0.0363 (12)
H25	0.278750	−0.136146	0.011676	0.044*

Atomic displacement parameters (Å^2)

	U^{11}	U^{22}	U^{33}	U^{12}	U^{13}	U^{23}
Re1	0.01419 (7)	0.01332 (8)	0.01797 (8)	0.00483 (5)	0.00064 (5)	0.00571 (6)
Br1	0.0246 (2)	0.0223 (2)	0.0326 (2)	−0.00051 (16)	0.00127 (17)	0.01517 (19)
Br3	0.0263 (2)	0.0235 (2)	0.0297 (2)	−0.00378 (17)	−0.00761 (17)	0.01230 (19)
Br2	0.0310 (2)	0.0401 (3)	0.0291 (2)	0.01602 (19)	0.00000 (18)	0.0194 (2)
P1	0.0150 (4)	0.0134 (5)	0.0177 (5)	0.0049 (4)	0.0009 (4)	0.0062 (4)
O12	0.0146 (12)	0.0169 (14)	0.0208 (14)	0.0042 (10)	0.0014 (10)	0.0080 (12)
O11	0.0169 (12)	0.0159 (14)	0.0154 (13)	0.0028 (10)	−0.0015 (10)	0.0047 (11)
O1	0.0290 (15)	0.0218 (16)	0.0288 (16)	0.0095 (12)	0.0039 (12)	0.0143 (14)
O2	0.0214 (14)	0.0255 (17)	0.0299 (17)	0.0053 (12)	−0.0087 (13)	−0.0036 (14)
O3	0.0257 (15)	0.0262 (17)	0.0289 (17)	0.0143 (13)	0.0026 (13)	0.0035 (14)
C1	0.0159 (17)	0.0114 (18)	0.0194 (19)	0.0050 (14)	−0.0008 (14)	−0.0020 (15)
C31	0.0162 (17)	0.019 (2)	0.0200 (19)	0.0062 (15)	0.0001 (15)	0.0089 (16)
C12	0.0185 (17)	0.0178 (19)	0.0171 (19)	0.0072 (15)	0.0048 (15)	0.0071 (16)
C16	0.0164 (17)	0.027 (2)	0.0183 (19)	0.0064 (16)	0.0005 (15)	0.0061 (17)
C13	0.0172 (17)	0.0157 (19)	0.025 (2)	0.0033 (15)	0.0046 (15)	0.0084 (17)
C11	0.0168 (17)	0.0148 (19)	0.0174 (18)	0.0076 (14)	0.0043 (14)	0.0055 (15)
C14	0.027 (2)	0.019 (2)	0.021 (2)	0.0117 (16)	0.0075 (16)	0.0091 (17)
C2	0.0187 (18)	0.019 (2)	0.026 (2)	0.0107 (15)	0.0068 (16)	0.0082 (17)
C15	0.0244 (19)	0.029 (2)	0.018 (2)	0.0148 (17)	0.0027 (16)	0.0107 (18)
C36	0.0175 (18)	0.020 (2)	0.023 (2)	0.0069 (15)	0.0027 (15)	0.0081 (17)
C3	0.0177 (18)	0.0146 (19)	0.021 (2)	0.0005 (15)	−0.0049 (15)	0.0050 (16)
C41	0.0205 (18)	0.0139 (18)	0.0164 (18)	0.0080 (14)	0.0016 (15)	0.0047 (15)
C17	0.0175 (17)	0.020 (2)	0.0189 (19)	0.0042 (15)	0.0043 (15)	0.0084 (16)
C21	0.0196 (18)	0.0157 (19)	0.0176 (19)	0.0059 (15)	0.0022 (15)	0.0015 (16)
C35	0.0216 (19)	0.020 (2)	0.028 (2)	0.0008 (16)	−0.0025 (17)	0.0091 (18)
C33	0.023 (2)	0.033 (3)	0.028 (2)	0.0106 (18)	0.0082 (17)	0.011 (2)
C32	0.0190 (18)	0.021 (2)	0.026 (2)	0.0090 (15)	0.0033 (16)	0.0075 (18)
C42	0.025 (2)	0.017 (2)	0.020 (2)	0.0060 (16)	0.0034 (16)	0.0052 (16)
C34	0.0167 (18)	0.027 (2)	0.033 (2)	0.0028 (16)	0.0049 (17)	0.016 (2)
C26	0.032 (2)	0.016 (2)	0.023 (2)	0.0014 (17)	0.0023 (17)	0.0064 (17)
C22	0.026 (2)	0.018 (2)	0.023 (2)	0.0070 (16)	−0.0014 (17)	0.0052 (17)
C45	0.027 (2)	0.042 (3)	0.043 (3)	0.018 (2)	0.001 (2)	0.018 (2)
C43	0.037 (2)	0.017 (2)	0.027 (2)	0.0114 (18)	0.0091 (19)	0.0071 (18)
C23	0.029 (2)	0.037 (3)	0.020 (2)	0.013 (2)	−0.0032 (17)	0.007 (2)

C24	0.030 (2)	0.036 (3)	0.023 (2)	−0.003 (2)	−0.0041 (18)	0.002 (2)
C46	0.0215 (19)	0.028 (2)	0.030 (2)	0.0097 (17)	0.0002 (17)	0.0144 (19)
C44	0.040 (2)	0.034 (3)	0.030 (2)	0.024 (2)	0.003 (2)	0.017 (2)
C25	0.049 (3)	0.018 (2)	0.032 (3)	0.001 (2)	0.007 (2)	0.004 (2)

Geometric parameters (Å, º)

Re1—C2	1.903 (4)	C41—C46	1.388 (5)
Re1—C1	1.917 (4)	C41—C42	1.399 (5)
Re1—C3	1.950 (5)	C21—C26	1.384 (6)
Re1—O12	2.127 (3)	C21—C22	1.395 (6)
Re1—O11	2.159 (2)	C35—C34	1.380 (7)
Re1—P1	2.4799 (11)	C35—H35	0.9500
Br1—C13	1.893 (4)	C33—C34	1.388 (7)
Br3—C17	1.889 (4)	C33—C32	1.390 (5)
Br2—C15	1.902 (4)	C33—H33	0.9500
P1—C41	1.820 (4)	C32—H32	0.9500
P1—C21	1.824 (4)	C42—C43	1.385 (6)
P1—C31	1.831 (4)	C42—H42	0.9500
O12—C12	1.276 (4)	C34—H34	0.9500
O11—C11	1.280 (4)	C26—C25	1.381 (6)
O1—C1	1.139 (5)	C26—H26	0.9500
O2—C2	1.148 (5)	C22—C23	1.374 (6)
O3—C3	1.140 (5)	C22—H22	0.9500
C31—C36	1.384 (6)	C45—C44	1.370 (6)
C31—C32	1.390 (6)	C45—C46	1.382 (6)
C12—C13	1.423 (5)	C45—H45	0.9500
C12—C11	1.464 (5)	C43—C44	1.381 (6)
C16—C15	1.381 (6)	C43—H43	0.9500
C16—C17	1.383 (5)	C23—C24	1.392 (7)
C16—H16	0.9500	C23—H23	0.9500
C13—C14	1.376 (5)	C24—C25	1.374 (7)
C11—C17	1.415 (5)	C24—H24	0.9500
C14—C15	1.377 (6)	C46—H46	0.9500
C14—H14	0.9500	C44—H44	0.9500
C36—C35	1.393 (5)	C25—H25	0.9500
C36—H36	0.9500		
C2—Re1—C1	86.27 (16)	C46—C41—P1	120.9 (3)
C2—Re1—C3	90.47 (17)	C42—C41—P1	120.1 (3)
C1—Re1—C3	88.72 (17)	C16—C17—C11	131.3 (4)
C2—Re1—O12	95.53 (14)	C16—C17—Br3	114.1 (3)
C1—Re1—O12	177.62 (13)	C11—C17—Br3	114.6 (3)
C3—Re1—O12	92.81 (14)	C26—C21—C22	119.4 (4)
C2—Re1—O11	167.93 (14)	C26—C21—P1	123.2 (3)
C1—Re1—O11	105.04 (13)	C22—C21—P1	117.1 (3)
C3—Re1—O11	93.90 (13)	C34—C35—C36	119.0 (4)
O12—Re1—O11	73.05 (10)	C34—C35—H35	120.5

C2—Re1—P1	91.16 (13)	C36—C35—H35	120.5
C1—Re1—P1	87.84 (12)	C34—C33—C32	119.7 (4)
C3—Re1—P1	176.09 (11)	C34—C33—H33	120.2
O12—Re1—P1	90.57 (8)	C32—C33—H33	120.2
O11—Re1—P1	85.20 (8)	C31—C32—C33	119.9 (4)
C41—P1—C21	107.08 (19)	C31—C32—H32	120.1
C41—P1—C31	104.34 (17)	C33—C32—H32	120.1
C21—P1—C31	103.82 (18)	C43—C42—C41	119.8 (4)
C41—P1—Re1	114.79 (13)	C43—C42—H42	120.1
C21—P1—Re1	112.03 (14)	C41—C42—H42	120.1
C31—P1—Re1	113.84 (15)	C35—C34—C33	121.0 (4)
C12—O12—Re1	118.7 (2)	C35—C34—H34	119.5
C11—O11—Re1	117.4 (2)	C33—C34—H34	119.5
O1—C1—Re1	178.2 (3)	C25—C26—C21	119.8 (4)
C36—C31—C32	119.8 (4)	C25—C26—H26	120.1
C36—C31—P1	120.4 (3)	C21—C26—H26	120.1
C32—C31—P1	119.8 (3)	C23—C22—C21	120.3 (4)
O12—C12—C13	118.8 (3)	C23—C22—H22	119.9
O12—C12—C11	115.3 (3)	C21—C22—H22	119.9
C13—C12—C11	126.0 (3)	C44—C45—C46	120.3 (4)
C15—C16—C17	128.9 (4)	C44—C45—H45	119.8
C15—C16—H16	115.5	C46—C45—H45	119.8
C17—C16—H16	115.5	C44—C43—C42	120.5 (4)
C14—C13—C12	131.7 (3)	C44—C43—H43	119.7
C14—C13—Br1	114.4 (3)	C42—C43—H43	119.7
C12—C13—Br1	113.8 (3)	C22—C23—C24	120.2 (4)
O11—C11—C17	120.4 (3)	C22—C23—H23	119.9
O11—C11—C12	115.1 (3)	C24—C23—H23	119.9
C17—C11—C12	124.5 (3)	C25—C24—C23	119.3 (4)
C13—C14—C15	127.6 (4)	C25—C24—H24	120.3
C13—C14—H14	116.2	C23—C24—H24	120.3
C15—C14—H14	116.2	C45—C46—C41	120.6 (4)
O2—C2—Re1	176.5 (4)	C45—C46—H46	119.7
C14—C15—C16	129.0 (4)	C41—C46—H46	119.7
C14—C15—Br2	115.3 (3)	C45—C44—C43	119.9 (4)
C16—C15—Br2	115.7 (3)	C45—C44—H44	120.1
C31—C36—C35	120.8 (4)	C43—C44—H44	120.1
C31—C36—H36	119.6	C24—C25—C26	121.0 (5)
C35—C36—H36	119.6	C24—C25—H25	119.5
O3—C3—Re1	175.8 (3)	C26—C25—H25	119.5
C46—C41—C42	118.8 (4)		

Hydrogen-bond geometry (Å, º)

D—H···*A*	*D*—H	H···*A*	*D*···*A*	*D*—H···*A*
C24—H24···O2^{i}	0.95	2.58	3.390 (5)	144
C26—H26···O1^{ii}	0.95	2.54	3.350 (5)	143
C36—H36···O11	0.95	2.52	3.299 (5)	139

C44—H44···Br3^{ii}	0.95	2.88	3.819 (4)	168
C46—H46···O3^{iii}	0.95	2.58	3.354 (5)	138

Symmetry codes: (i) $-x$, $-y$, $-z$; (ii) x, $y-1$, z; (iii) $x+1$, y, z.